Optics Communications 354 (2015) 414–418

Contents lists available at ScienceDirect

Optics Communications

journal homepage: www.elsevier.com/locate/optcom

High energy 523 nm ND:YLF pulsed slab laser with novel pump beam waveguide design

Qi Yang [a,b], Xiaolei Zhu [a,*], Jian Ma [a], Tingting Lu [a], Xiuhua Ma [a], Weibiao Chen [a]

[a] *Key Laboratory of Space Laser Communication and Detection Technology, Shanghai Institute of Optics and Fine Mechanics, Chinese Academy of Sciences, Shanghai 201800, China*
[b] *University of Chinese Academy of Sciences, Beijing 100049, China*

ARTICLE INFO

Article history:
Received 19 April 2015
Received in revised form
8 June 2015
Accepted 10 June 2015
Available online 12 June 2015

Keywords:
Diode-pumped
Q-switched
Laser amplifiers

ABSTRACT

A laser diode pumped Nd:YLF master oscillator power amplifier (MOPA) green laser system with high pulse energy and high stable output is demonstrated. At a repetition rate of 50 Hz, 840 mJ pulse energy, 9.1 ns pulse width of 1047 nm infrared laser emitting is obtained from the MOPA system. The corresponding peak power is 93 MW. Extra-cavity frequency doubling with a LiB_3O_5 crystal, pulse energy of 520 mJ at 523 nm wavelength is achieved. The frequency conversion efficiency reaches up to 62%. The output pulse energy instability of the laser system is less than 0.6% for one hour.

1. Introduction

Solid-state green lasers with high pulse energy and high beam quality have been rapidly developed recently. Green lasers perform better than IR lasers in many applications, such as large-area material treatment, precision micro-fabrication and underwater communication. Even more, high energy green lasers can be used to pump Ti:sapphire lasers and generate UV lasers. Compared with lamp-pumped solid-state green lasers, the diode-pumped system is reliable, efficient and stable. Traditionally, extra-cavity frequency doubling is a widely used method to obtain high energy green pulse for a master oscillator power amplifier (MOPA) system [1–4]. In 2000, Hirano et al. designed an external two-stage KTP crystal architecture. The system produced 131 W average power in green with a frequency conversion efficiency as high as 65.2%, and the beam quality factor M^2 was around 5.2 [1]. Using an external KTP crystal, Kiriyama demonstrated 132 W of green pulse train output at 1 kHz, and the frequency conversion efficiency was 60% [2]. In a high power Q-switched $Nd:YVO_4$ MOPA system, Liu demonstrated 103.5 W of 532 nm wavelength laser output [3]. In 2013, Li reported a single-frequency Nd:YAG MOPA system with extra-cavity frequency doubling; at a repetition rate of 250 Hz, 532 nm green laser with 12.6 ns pulse width and 400 mJ pulse energy was obtained [4].

Nd:YLF, as a high quality fluoride, has been proven a very good laser crystal to generate high energy laser. The laser transition of Nd:YLF is at 1047 nm (extraordinary) or at 1053 nm (ordinary); therefore the wavelength of second harmonic generation (SHG) is closer to the spectral window of sea water than 532 nm obtained from Nd:YAG lasers [5]. Nd:YLF material has other advantages, such as long fluorescence lifetime (480 µs), natural birefringence and low thermal effect. The main challenge of Nd:YLF crystal for high energy laser application is its small tensile strength (33 MPa), which critically limits the maximum average pump power density. In 1993, Beach demonstrated a diode-end-pumped Nd:YLF laser emitting at 1047 nm wavelength, 100 mJ of pulse energy with 4 ns pulse width was obtained, and the repetition rate was 30 Hz [6]. In 1998, Clarkson reported a Nd:YLF laser at 1053 nm wavelength, pumped by two beam-shaped 20 W diode bars. The pulse energy was around 2.6 mJ at a repetition frequency of 1 kHz [7]. In 2004, Q-Peak company demonstrated a high-repetition rate Nd:YLF MOPA system; 45 W green light was achieved, but the pulse energy was low [8]. Similarly, Li reported a stable–unstable hybrid resonator Nd:YLF laser in 2008, and 15.1 mJ pulse energy with 7.1 ns pulse width at 523 nm wavelength was achieved [9]. Lu also designed a diode-end-pumped, conductively cooled intra-cavity frequency doubling Nd:YLF lasers for 527 nm or 523 nm output [10,11]. But until now, high energy diode-pumped 523 nm Nd:YLF green lasers have rarely been reported.

In this paper, we demonstrate a conductively cooled, high pulse energy Nd:YLF green laser at 523 nm. A MOPA system was used to generate 1047 nm fundamental wavelength, and a LiB_3O_5 (LBO) crystal was used for extra-cavity frequency doubling. Two

* Corresponding author.
E-mail address: xlzhu@siom.ac.cn (X. Zhu).

http://dx.doi.org/10.1016/j.optcom.2015.06.022
0030-4018/

cylindrical lenses were employed to compensate the thermal lens effect in two different directions. The MOPA system provided output energy of 840 mJ with pulse duration of 9.1 ns. Using extra-cavity frequency doubling method, 520 mJ pulse energy at 523 nm wavelength was achieved with 62% frequency conversion efficiency.

2. Experimental setup

The schematic of the experimental setup is shown in Fig. 1. The system consists of three parts, an EO Q-switched oscillator, Nd:YLF slab amplifiers and a frequency conversion stage. A U-type arrangement of the oscillator [11] could make the construction compact. The gain material was a pair of a-cut Nd:YLF crystal slabs (1.0 at.% Nd^{3+}-doped), the dimension of each crystal was $4\times4\times12$ mm^3. Total 24 mm slab in length was designed to absorb the pump energy completely. The crystals were end-pumped by two fiber coupled QCW 806 nm laser diodes operated at 50 Hz repetition rate with 480 μs pulse duration. The folded resonator consisted of a high-reflectivity mirror M1 with curvature radius of 2000 mm; two flat, high-reflectivity mirrors M2 and M3 ($R>99.8\%$ at 1047 nm, high transmission at 806 nm), and a flat output coupler M4 with a transmission of 60% at 1047 nm. The total cavity length was 620 mm. A KD*P Pockel cell, a polarizer, and a quarter wave plate were used as the electro-optic Q-switcher.

The amplification stage involved two pre-amplifiers and two power-amplifiers. For every amplifier head, LD pumping and cooling architecture is shown in Fig. 2. The pump sources were quasi-cw diode stacks; each stack consisted of four 10 mm long diode bars (pre-amplifier) or six 10 mm long diode bars (power-amplifier). The maximum peak power of each LD bar was 150 W at the central wavelength of 806 nm. The full divergence angles in the fast and slow axes were approximately 40° and 10°. The pumping LD operated at a repetition rate of 50 Hz, with a pulse width of 400 μs. Six LD stacks were arranged in each pre-amplifier, 10 LD stacks were arranged in power-amplifier-1, and 11 LD stacks were adopted in power-amplifier-2. The LD stacks were staggered at two sides of each slab. In order to suppress parasitic oscillation, the Nd:YLF slabs were cut to 3° angle. For the sake of increasing the absorbing efficiency, 1 at.% concentration of Nd^{3+} was chosen. Considering the damage threshold of the crystal and the fluence of the signal, the beam sizes of the signal were controlled at 4.5×4.5 mm^2, 6×6 mm^2 and 8×8 mm^2 respectively by expansion telescope. In order to increase the overlap efficiency and decrease the diffraction effect, slabs with size of $6\times6\times72$ mm^3 were used in the pre-amplifiers, one $8\times\ 8\times110$ mm^3 slab was used in the power-amplifier-1, and a $10\times10\times120$ mm^3 slab was used in the power-amplifier-2.

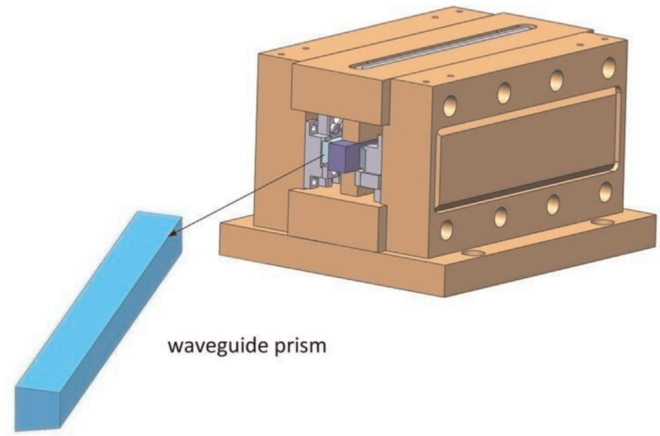

Fig. 2. Schematic of the amplifier head.

As we known, the main challenges involved in an LD array are its highly divergent output and large beam divergence. These drawbacks lead to the irregular and non-uniform output radiation of LD array. To overcome these problems, many researchers have applied lens ducts to shape the pumping beam [12,13], but the coupling efficiency of lens ducts is low, and the size is large. We therefore designed a trapezoid waveguide prism to couple the pump laser. The structure configuration of the waveguide prism is also shown in Fig. 2. The dimension of the waveguide prism was accurately calculated by ray tracing method. The height of the

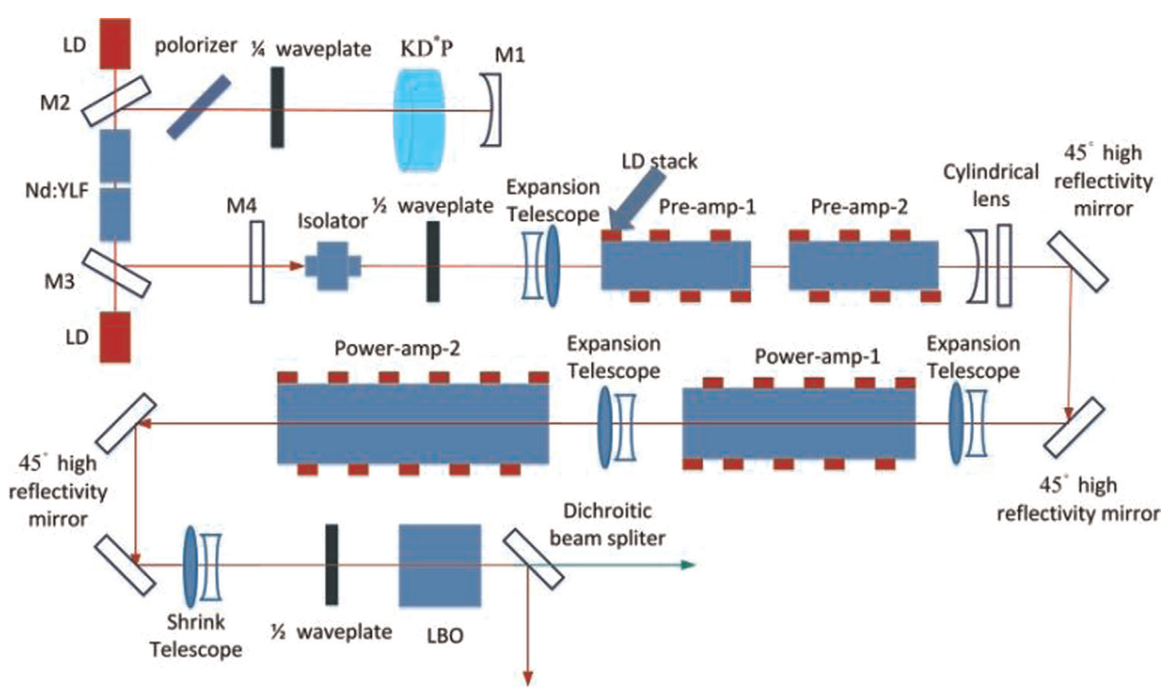

Fig. 1. Schematic of the experimental setup.

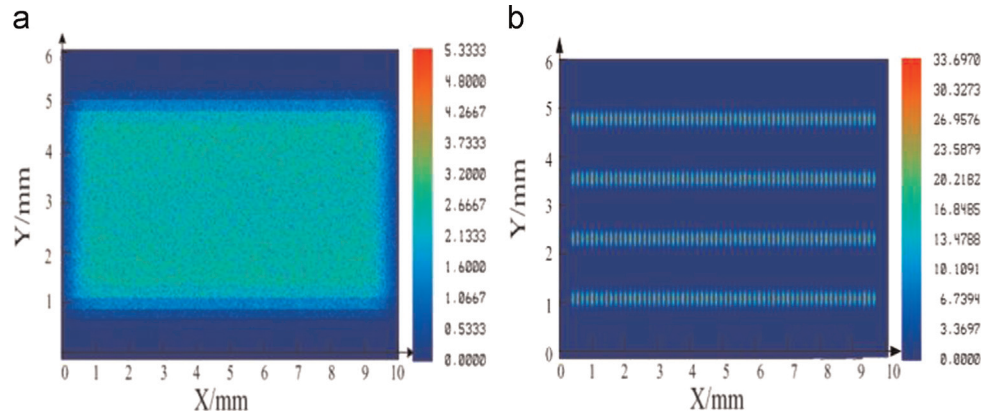

Fig. 3. Pump beam intensity distribution (a) with waveguide in front of the slab; and (b) without waveguide in front of the slab.

waveguide prism was 5 mm for pre-amplifier and 6 mm for power-amplifier. The space between the waveguide prism and the emission surface of LD array, as well as the space between the waveguide prism and the slabs was less than 1 mm. For the pre-amplifiers, the bottom width of the trapezoid waveguide prism was 5 mm, and the top width was 4 mm. For the power-amplifier-1, the bottom width was 7 mm, and the top width was 6 mm. For the power-amplifier-2, waveguide prism with 9 mm in bottom width and 8 mm in top width was designed. This design makes the coupling system compact, and approximately 99% coupling efficiency was achieved, which was greatly larger than that of the lens ducts. A typically simulated intensity distribution of pumping beam in front of Nd:YLF slab pumping-surface of the pre-amplifier with the waveguide prism and without any coupling system are shown in Fig. 3. It is believed that, using the waveguide prism, the pump beam intensity distribution in the gain medium would perform quite uniform and concentrated. Similar simulated results were also obtained for the power-amplifiers.

The thermo-optical coefficient of Nd:YLF is negative. Some previous works revealed that the thermal effect of Nd:YLF was weaker than that of Nd:YAG, and the thermal lens of Nd:YLF in π-polarization was negative [14,15]. In our experiments, the thermal lens in vertical direction was negative, but in horizontal direction was positive. It was believed that this result was due to the special cooling architecture, as shown in Fig. 2. The thermal gradient in vertical direction was larger than that in horizontal direction. Finally, the effect of end-face curvature of the slab in horizontal direction was more serious than the effect of thermal induced refractive index changing, and positive thermal lens was induced. So, two cylindrical lenses were used to compensate the thermal lens effect of slab.

A type-I phase-matched LBO crystal ($12 \times 12 \times 15$ mm^3, $\theta=90°$, $\varphi=11°$), anti-reflectivity coated at 523 nm and 1047 nm wavelength, was used for extra-cavity frequency doubling. A telescope with an amplification of 0.5 was employed to improve the laser power density inside the nonlinear crystal. The focused laser beam dimension in the LBO crystal was around 4×4 mm^2, so the laser power density was up to 577 MW/cm^2. The fundamental and second harmonic beams after LBO were separated by a dichroitic beam splitter (HT@523 nm, HR@1047 nm).

3. Experimental results

With 65 mJ pump pulse energy, 13 mJ pulse energy at 1047 nm wavelength was produced from the Q-switched Nd:YLF oscillator, and the optical to optical efficiency was around 20%. The beam quality factors were $M_x^2 = 1.26$, and $M_y^2 = 1.47$. Fig. 4(a) depicts the typical Q-switched pulse profile with 13.7 ns pulse duration. The output pulses from the master oscillator were then amplified by a four-stage side-pumped amplifier. The amplified pulse energy as a function of absorbed pump energy is depicted in Fig. 5. The maximum output pulse energy of 840 mJ was extracted from the amplifier chain while the input signal energy was around 13 mJ per pulse, with the total absorbed pump pulse energy around 6.6 J. The optical to optical conversion efficiency of the pre-amplifiers was 5.7%; efficiency of the first power-amplifier was 11.8%, and efficiency of the second power-amplifier was 17.3%. The total optical conversion efficiency was 12.5%.

Based on the Frantz–Nodvik equation [16,17], the amplified pulse energy E_{out} as a function of input signal pulse energy E_{in} can be simulated as following:

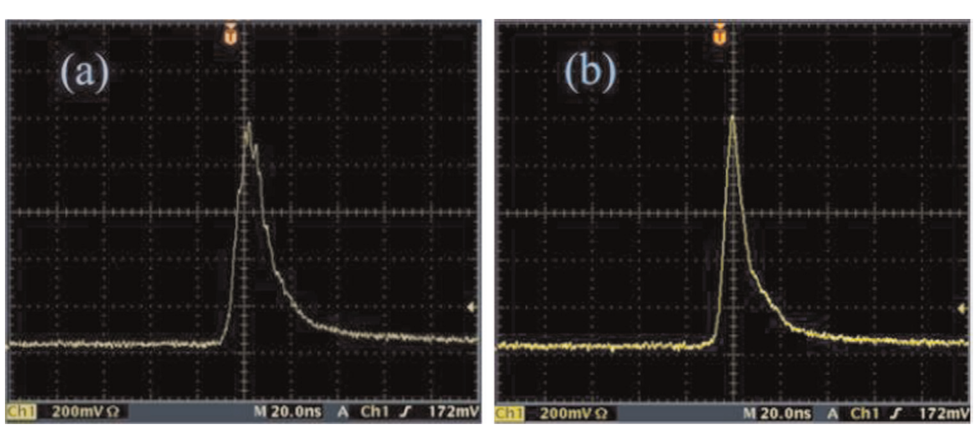

Fig. 4. Temporal trace of laser pulse. (a) Pulse from the oscillator; and (b) pulse from the amplifier.

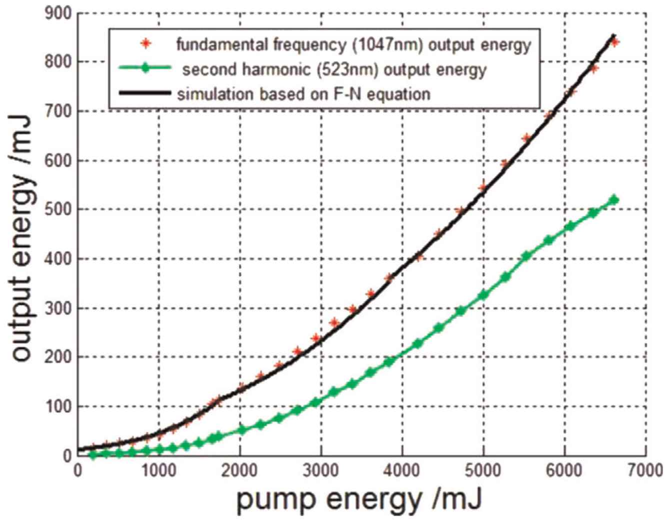

Fig. 5. 1047 nm and 523 nm pulse output energy as a function of the absorbed pump energy.

$$E_{out} = E_s A\left\{1 + \left[\exp\left(\frac{E_{in}}{AE_s}\right) - 1\right]\exp\left(g_0 L\right)\right\}, \tag{1}$$

where E_s is the saturation fluence of Nd:YLF crystal at 1047 nm wavelength (E_s = 1.05 J/cm^2), g_0 is the small-signal gain coefficient, A is the area of the beam and L is the effective crystal length.

$$g_0 L = \frac{\eta_s \eta_Q \eta_B \eta_{st} \eta_{ASE} E_P}{AE_s} \tag{2}$$

where η_s is the Stokes efficiency, η_Q is the quantum efficiency, η_B is the beam overlap efficiency, η_{st} is the storage efficiency, η_{ASE} is the amplified spontaneous emission efficiency, E_P is the absorbed pump pulse energy.

The simulation results are also shown in Fig. 5, which meet the experimental results well. At the beginning, the output pulse energy increased with the pump energy exponentially, and then increased linearly. No saturation amplification was observed in the range of pumping energy. As the maximum output energy was approached, the experimental value became less than the simulation value. It is believed that more serious thermal effect induced by high pump energy resulted in low efficiency. The amplified pulse with duration of 9.1 ns was detected and shown in Fig. 4(b), and its peak power of the amplified pulse was around 93 MW. In this experiment, saturation amplification did not appear yet, so the pulse duration got shorter than that of signal pulse. To evaluate the spatial distribution of the laser beam, the beam quality was measured. On the condition of 840 mJ pulse energy output, the beam quality factors of $M_x^2 = 3.26$, $M_y^2 = 4.29$ were recorded, as shown in Fig. 6, and the degree of polarization of the laser beam was about 99%. In order to improve the beam quality, the dimension of the slabs and the focal length of the cylindrical lenses should be further optimized. The far-field beam intensity distribution profile after amplification is shown in Fig. 7. The intensity of the beam was well-distributed but became non-Gaussian in shape because of the high-order thermal aberration due to the non-uniform pumping and cooling.

In the experiment, an LBO crystal was used for the extra-cavity frequency doubling. The pulse energy of green light as a function of incident pump energy is also shown in Fig. 5. The maximum pulse energy of 520 mJ was obtained. The frequency conversion efficiency was up to 62%. The central wavelength was about 523.5 nm, and the pulse width was around 8.0 ns. Fig. 8 shows the output green laser pulse energy variation over 1 h recorded by the energy meter. Less than 0.6% of the green laser pulse energy fluctuation was finally derived based on one hour measurement data. It could safely operate without any damage occurred on the

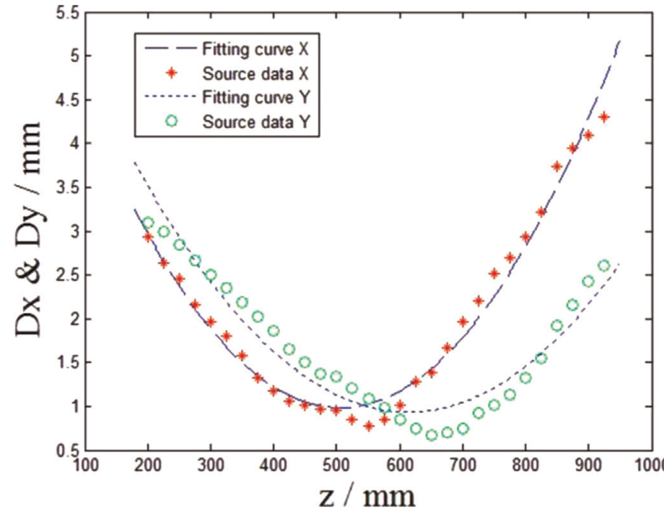

Fig. 6. Beam quality of the MOPA system (D_x, D_y represent the beam diameter in horizontal and vertical directions).

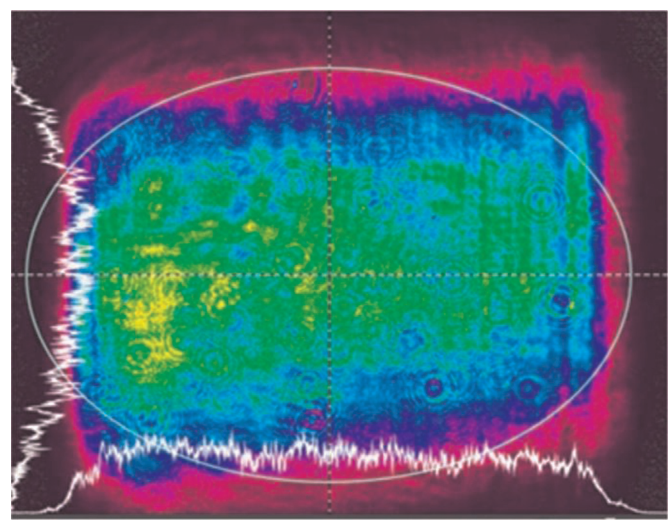

Fig. 7. Far-field beam intensity distribution after amplification.

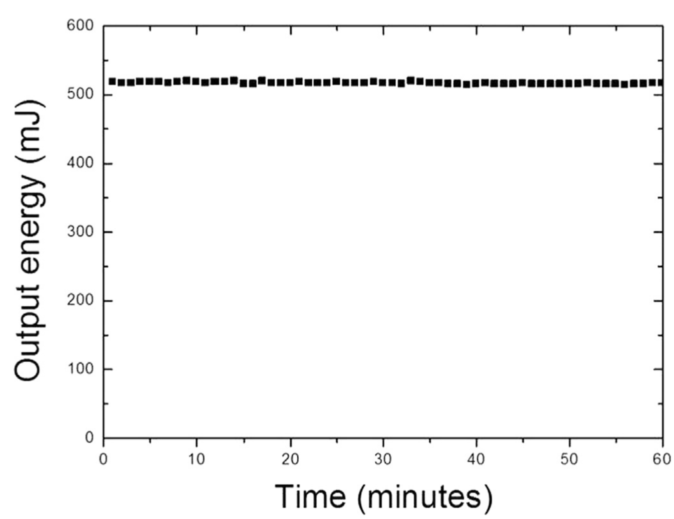

Fig. 8. 523 nm laser pulse energy stability over 1 h.

condition of maximum output.

4. Conclusion

In conclusion, we proposed a stable and high energy Nd:YLF 523 nm green laser system. At the repetition rate of 50 Hz, the maximum pulse energy of 523 nm green laser output was 520 mJ. The extra-cavity frequency conversion efficiency reached 62%. To our knowledge, this is the highest energy output for diode-pumped Nd:YLF pulsed slab laser at 523 nm wavelength. The output pulse energy fluctuation was measured to be less than 0.6%. This high energy and stable output green laser can be used in long distance underwater communication.

References

[1] Y. Hirano, N. Pavel, S. Yamamoto, Y. Koyata, T. Tajime, Opt. Commun. 184 (2000) 231–236.
[2] H. Kiriyama, K. Yamakawa, T. Nagai, Opt. Lett. 28 (2003) 1671–1673.
[3] Q. Liu, X. Yan, M. Gong, X. Fu, D. Wang, Opt. Express 16 (2008) 14335–14340.
[4] S. Li, X. Ma, H. Li, F. Li, X. Zhu, W. Chen, Chin. Opt. Lett. 11 (2013) 071402.
[5] M. Lanzagorta, Underwater Communications, Morgan & Claypool Publishers, San Rafael, California, USA, 2012.
[6] R. Beach, P. Reichert, W. Benett, B. Freitas, S. Mitchell, A. Velsko, J. Davin, R. Solarzm, Opt. Lett. 18 (1993) 1326–1328.
[7] W.A. Clarkson, P.J. Hardman, D.C. Hanna, Opt. Lett. 23 (1998) 1363–1365.
[8] A. Dergachev, P.F. Moulton, Advanced solid-state photonics, OSA Trends in Optics and Photonics, paper 191, 2004.
[9] D. Li, Z. Ma, R. Haas, A. Schell, P. Zhu, P. Shi, K. Du, Opt. Lett. 33 (2008) 1708–1710.
[10] T. Lu, J. Wang, M. Huang, D. Liu, X. Zhu, Chin. Opt. Lett. 10 (2012) 081403.
[11] T. Lu, J. Ma, M. Huang, Q. Yang, X. Zhu, W. Chen, Chin. Phys. Lett. 31 (2014) 074208.
[12] R. Fu, G. Wang, Zi Wang, E. Ba, G. Mu, X. Hu, Appl. Opt. 37 (1998) 4000–4003.
[13] G. Feugnet, C. Bussac, C. Larat, M. Schwarz, J.P. Pocholle, Opt. Lett. 20 (1995) 157–159.
[14] C. Pfistner, R. Weber, H.P. Weber, S. Merazzi, R. Gruber, IEEE J. Quantum Electron. 30 (1994) 1605–1615.
[15] P.J. Hardman, W.A. Clarkson, G.J. Friel, M. Pollnau, D.C. Hanna, IEEE J. Quantum Electron. 35 (1999) 647–655.
[16] L.M. Frantz, J.S. Nodvik, J. Appl. Phys. 34 (1963) 2346–2349.
[17] P. Peuser, W. Platz, P. Zeller, T. Brand, M. Haag, B. Köhler, Opt. Lett. 31 (2006) 1991–1993.